Aalto University

OPEN ACCESS

This is an electronic reprint of the original article.
This reprint may differ from the original in pagination and typographic detail.

Sundaria, Ravi; Lehikoinen, Antti; Hannukainen, Antti; Arkkio, Antero; Belahcen, Anouar

Mixed-Order Finite-Element Modeling of Magnetic Material Degradation Due to Cutting

Published in:
IEEE Transactions on Magnetics

DOI:
10.1109/TMAG.2018.2811385

Published: 01/01/2018

Document Version
Peer-reviewed accepted author manuscript, also known as Final accepted manuscript or Post-print

Please cite the original version:
Sundaria, R., Lehikoinen, A., Hannukainen, A., Arkkio, A., & Belahcen, A. (2018). Mixed-Order Finite-Element Modeling of Magnetic Material Degradation Due to Cutting. *IEEE Transactions on Magnetics*, *54*(6), Article 7402008 . https://doi.org/10.1109/TMAG.2018.2811385

This material is protected by copyright and other intellectual property rights, and duplication or sale of all or part of any of the repository collections is not permitted, except that material may be duplicated by you for your research use or educational purposes in electronic or print form. You must obtain permission for any other use. Electronic or print copies may not be offered, whether for sale or otherwise to anyone who is not an authorised user.

Mixed Order Finite Element Modeling of Magnetic Material Degradation Due to Cutting

Ravi Sundaria[1], Antti Lehikoinen[1], Antti Hannukainen[2] Antero Arkkio[1], and Anouar Belahcen[1]
[1]Department of Electrical Engineering and Automation, Aalto University, Espoo, 15500, Finland
[2]Department of Mathematics and System Analysis, Aalto University, Espoo, 11100, Finland

As a part of manufacturing of electrical machines, electrical sheets are cut to the desired shape by various cutting techniques such as punching, laser cutting etc. This cutting process degrades the magnetic material near the cut-edge which should be included in the finite element modeling of electrical machines. However, due to the nature of the cutting effects, the existing finite element modeling of the cutting effect results in computationally heavy simulations. This paper investigates the application of mixed order elements to model the cutting effect. The second order nodal triangular elements are used near the cut-edge whereas transition/first order elements are applied in the remaining solution domain. Further, the accuracy of the presented method is analyzed with the traditional method. According to the simulations, the mixed order elements returned accurate results significantly faster than the traditional finite element based approaches. Further, the effect of the cutting on the machine performance is also studied by comparing it's results briefly.

***Index Terms*—Core loss, cutting, cut edge, electrical machines, finite element modeling, mixed order elements, punching, steel laminations.**

I. Introduction

ELECTRICAL machines are extensively used in electrical power generation and as conversion devices. Therefore, the government regulations around the world are encouraging the usage of better efficiency machines and electrical designers need to develop more optimized machines with lower losses. One of the loss component, which is often neglected at the design stage of an electrical machine are the losses due to the cutting of electrical sheets. These losses present significant challenges in terms of available standard loss models, computational cost etc. Clearly, a computationally efficient approach may encourage the future machine designers to study these losses and thus help in developing higher efficiency electrical machines.

The material degradation due to the cutting of electrical sheets is justified by various techniques. Electron backscatter diffraction (EBSD), optical microscope [1] and, micro hardness measurements [2] confirm the distortion in the grains of magnetic material near the cut edge. The degradation of magnetic material properties such as magnetic excitation and core losses are further measured by experiments [3], [4]. To include this degradation phenomenon in the electrical machine design process various authors developed associated loss models. Researchers have presented analytical loss models [5] as well as finite element based loss models [3], [6], [7]. The effect of the magnetic material degradation in different parts of a machine such as the stator teeth and yoke was considered by building factors [8] or by different magnetization curves [3]. Among the finite element based loss models, the effect of degradation is either quantified by a single degraded material layer near the cut edge [9], [10] or by many such layers [6], [7]. Many degraded layers present a gradual progression of the magnetic material degradation near the cut edge, which is also closer to the actual physical phenomenon. However, the resultant computational model becomes quite heavy for any practical purpose.

Recently, the authors of [11] studied the application of higher order elements to reduce the computation burden of the inclusion of cutting related effects. However, this approach will generate higher order elements in all the parts of electrical machines which may not be required such as the air gap, the stator slots, the rotor bars etc. Therefore, this paper analyses the mixed order elements for modeling the cutting effect; i.e. higher order elements near the cut edge and usually used linear elements in the other parts of electrical machine.

The application of the mixed order finite elements is well established in the mathematical finite element literature [12], [13]. The mixed order elements are also applied in different engineering domains [14], [15]. These elements are especially beneficial when we have to model a specific phenomenon in certain part of the solution domain efficiently. The developed loss model related to cutting presents a high degree of variation in permeability near the cut edge, which is normally represented by parabolic or exponential functions [6], [7]. However, it is observed that the cutting effect is negligible after 5-10 mm distance from the cut-edge. Therefore, the application of higher order elements in unaffected areas of iron can be avoided by the application of mixed order elements.

This paper first reviews the theory of mixed order elements and describes the required shape/basis functions of the presented finite element formulation. Further, suitable mixed order elements are selected based on the loss model presented in [11]. The accuracy of the mixed order elements is then compared with a highly dense first order mesh. Two cases are considered; a time stepping analysis of a stator tooth and a time harmonic model of a cage induction machine at different loads. At last, the benefits in terms of computational efficiency of the presented mixed order finite element formulation is discussed in comparison with the traditional method.

Manuscript received September X, 2017; revised January X, 2018. Corresponding author: R. Sundaria (email: ravi.sundaria@aalto.fi).

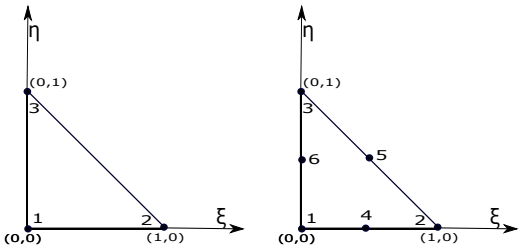

(a) (b)

Fig. 1. (a) First order reference element (b) Second order reference element.

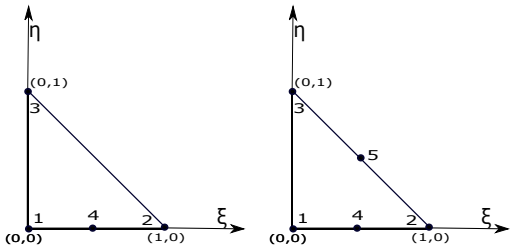

(a) (b)

Fig. 2. (a) Transition reference element 1 (T_{e1}) (b) Transition reference element 2 (T_{e2}).

II. Method

This section is divided into two parts; the first part deals with the theory of mixed order elements, whereas the second part presents the application of the mixed order elements in the finite element model of electrical machines.

A. Mixed order elements

The order of a finite element represents the polynomial order of the associated variable. Therefore, first order elements represent linear shape functions, second order elements deal with shape functions of a polynomial degree two and so on. For most of the finite element based applications, a uniform order of the elements is maintained in the entire solution domain due to relatively easier implementation and solution requirements. However, some specific applications may demand mixed order elements i.e. two or more different types of elements in the same solution domain. This paper will study the application of mixed, second order and first order elements in a solution domain. As the associated finite element variable needs to be continuous at transition between second and first order elements; different shape function will be used for these transition elements.

As per the theory of the nodal shape functions; every nodal shape function should attain a value 1 with the associated node whereas it should attain a value zero at all other nodes in the domain. Based on this criterion, the shape functions of first order reference element (Fig. 1a) are N_1^1, N_2^1 and, N_3^1 in the ξ η reference frame and are presented in (1). Similarly, the shape functions of second order reference element Fig. 1b are described in (2).

$$N_1^1 = 1 - \xi - \eta \qquad N_2^1 = \xi \qquad N_3^1 = \eta \tag{1}$$

$$\begin{aligned} N_1^2 &= N_1^1 - 0.5N_4^2 - 0.5N_6^2 & N_4^2 &= 4(1-\xi-\eta)\xi \\ N_2^2 &= N_2^1 - 0.5N_4^2 - 0.5N_5^2 & N_5^2 &= 4\xi\eta \\ N_3^2 &= N_3^1 - 0.5N_5^2 - 0.5N_6^2 & N_6^2 &= 4(1-\xi-\eta)\eta \end{aligned} \tag{2}$$

However, as stated earlier, special shape functions are needed in the case of transition elements. Two types of transition elements are possible in this case of second and first nodal mixed order elements. Either a transition element has one edge linked with second order element and the other two are with the first order elements or vice-versa. This paper terms these transition elements as T_{e1} and T_{e2} . As presented in Fig. 2, T_{e1} contains 4 nodes whereas T_{e2} contains 5 nodes in an element. The corresponding reference shape functions are described in (3) and (4) respectively. The application of transition elements will ensure the continuity of the global shape function in the solution domain. Further, for better understanding, the behaviour of the shape functions of the transition element T_{e1} are plotted in Fig. 3 as an example. As the edge containing nodes 1, 4 and, 2 in T_{e1} is also associated with a second order element, the corresponding shape functions have polynomial order of 2. Moreover, the same can be interpreted for T_{e2}.

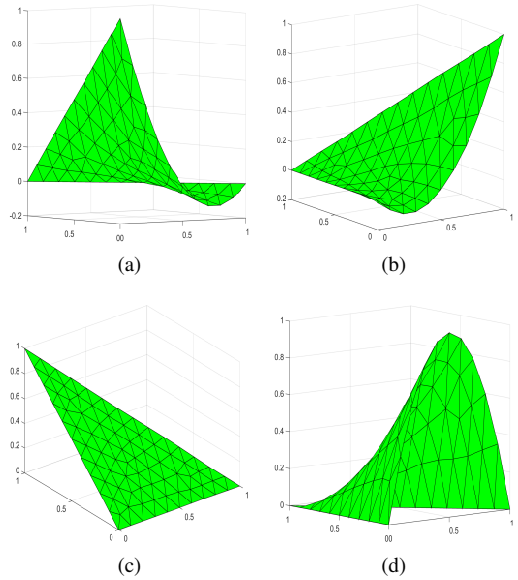

(a) (b) (c) (d)

Fig. 3. (a) Shape function $N_1^{T_{e1}}$ (b) Shape function $N_2^{T_{e1}}$ (c) Shape function $N_3^{T_{e1}}$ (d) Shape function $N_4^{T_{e1}}$.

$$\begin{aligned} N_1^{T_{e1}} &= N_1^1 - 0.5N_4^2 & N_3^{T_{e1}} &= N_3^1 \\ N_2^{T_{e1}} &= N_2^1 - 0.5N_4^2 & N_4^{T_{e1}} &= N_4^2 \end{aligned} \tag{3}$$

$$\begin{aligned} N_1^{T_{e2}} &= N_1^1 - 0.5N_4^2 & N_4^{T_{e2}} &= N_5^2 \\ N_2^{T_{e2}} &= N_2^1 - 0.5N_4^2 - 0.5N_5^2 & N_5^{T_{e2}} &= N_4^2 \\ N_3^{T_{e2}} &= N_3^1 - 0.5N_5^2 \end{aligned} \tag{4}$$

B. Higher order finite element with material degradation

This paper uses the measurement results and the cut-edge dependent material model described in [11]. The effect of cutting on the magnetic permeability of the material depends primarily on two parameters: the cut-edge distance and the magnetic field strength (magnetic saturation). The cut distance dependent permeability function is presented in (5).

$$\mu(H,x) = \mu_{\text{nd}}(H)(1 - e^{-ax}e^{-bH}) \tag{5}$$

$$p(B(H,x),x) = c(1 + e^{-dx})B^2(H,x) \tag{6}$$

The permeabilities of the degraded and nondegraded iron material are denoted by μ and μ_{nd} respectively. x is the cut distance and H is the magnetic field strength. As the magnetic field strength is assumed constant across the width of lamination; the multiplication of H with (5) will provide local magnetic flux density. Similarly, the cut-edge dependent specific core loss density is presented in (6). Here $B(H,x)$ is local magnetic flux density with fitting parameters c and d. Moreover with the Epstein frame, the average magnetic flux density and average loss density are measured. Therefore the cut-edge dependent local functions in (5) and (6) need to be averaged across the width of the lamination samples. The fitting parameters are then obtained with the help of the nonlinear least-square solver of MATLAB. For the given experimental test, data fitting parameters $a = 795$ (1/m), $b = 0.001664$ (A/m), $^{-1}$ $c = 0.835$ (W/kg T^2) and, $d = 925$ (1/m) are obtained.

The application of third order nodal triangular elements to model the cutting effect is also presented in detail in [11]. In a similar fashion, the stiffness matrix $\mathbf{S}$ in the magnetic vector potential based AV finite element formulation will be modified as presented in (7). The source vector is presented as $\mathbf{f}$.

$$\mathbf{S}(\mathbf{A},x)\mathbf{A} = \mathbf{f} \tag{7}$$

The entries of the stiffness matrix S_{ij} can be represented in terms of the reluctivity ν and the nodal shape functions ϕ in the domain Ω. The effect of cutting in terms of the degradation of permeability from (5) is presented in the form of the cut distance dependent reluctivity $\nu(A,x)$. The numerical integration in (8) is performed with the help of the Gaussian quadrature and for convenience the same number of integration points are used in the second order and transition elements.

$$S_{ij}(A,x) = \int_{\Omega} \nu(A,x)\nabla\phi_i \cdot \nabla\phi_j d\Omega \tag{8}$$

C. FEM implementation

A time stepping analysis of a stator tooth and a time-harmonic analysis of a cage induction machine are presented in this paper. The finite element analysis code with three different types of elements (first, third and mixed order) is written in MATLAB environment. A voltage source time harmonic model for cage induction machine is used [16], [17]. The effect of the stator end winding impedances is taken into account with the help of circuit equations and the rotor bars are considered as short circuited. The nonlinearity in iron

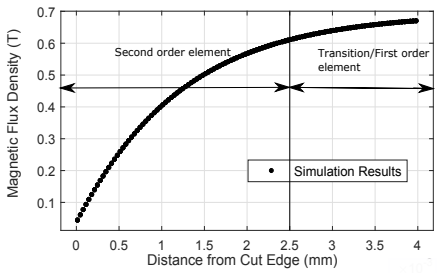

Fig. 4. Behavior of magnetic flux density near the cut edge with applied magnetic flux density of 0.5 T and the selection of appropriate order of finite elements near the cut edge

are handled with the Newton-Raphson method and the eddy currents are not considered in the iron laminations during the field simulation. The resultant nonlinear system of equations is presented in (9).

$$\begin{bmatrix} \mathbf{S} + \tilde{\mathbf{M}} & (\mathbf{D}^s)^T\mathbf{K}^T \\ \mathbf{K}\mathbf{D}^s & \tilde{\mathbf{G}}^s \end{bmatrix} \cdot \begin{bmatrix} \tilde{\mathbf{A}} \\ \tilde{\mathbf{i}}^s \end{bmatrix} = \begin{bmatrix} 0 \\ -\tilde{\mathbf{V}}^s \end{bmatrix} \tag{9}$$

Here, the magnetic vector potential $\tilde{\mathbf{A}}$ and the supply current $\tilde{\mathbf{i}}^s$ are unknowns and the symbol $\tilde{}$ denote the complex nature of the matrices. Further, $\mathbf{S}$ and $\tilde{\mathbf{M}}$ are the stiffness and mass matrices. The stator flux linkage is represented by the matrix $\mathbf{D}^s$. Moreover, the stator winding impedance is included in the form of the matrix $\tilde{\mathbf{G}}^s$ with $\tilde{\mathbf{V}}^s$ is the voltage source . The effect of cutting will be reflected in the stiffness matrix $\mathbf{S}$ which is assembled as per (8).

III. Results

A. Selection of mixed order elements

The behaviour of the magnetic flux density near the cut edge was analyzed in [11]. The distribution of the magnetic flux density near the cut-edge depends on the distance from the cut edge as well as the magnetic field. The major effect happens between magnetic field strengths 50 A/m to 1000 A/m. Fig. 4 represents the magnetic flux density distribution near the cut edge when the average magnetic flux density of 0.5 T was enforced. Based on this flux density distribution a separate geometric region of 2.5 mm width can be introduced near the cut edge, which will represent the degraded material due to the cutting. Further analyzing the flux distribution and ease of implementation of the mixed order elements in the finite element tool, it was decided that the second order elements will be applied in the degraded region. Moving away from the cut edge, adjacent to second order elements, there will be transition elements. Thereafter, first order elements will be applied in the rest of the domain.

B. Accuracy of mixed order elements

The accuracy of the mixed order elements is analyzed by comparing a highly dense first order mesh. A cage induction motor stator tooth was selected as an example. First, 2-D time stepping finite element analysis of the cage induction machine was carried out without considering the cutting effect. Afterwards, a stator tooth was extracted for the study of the cutting

TABLE I
MESH DATA

Mesh	Elements	Nodes
First Order	4328	2256
Third order	68	343
Mixed order	211	265

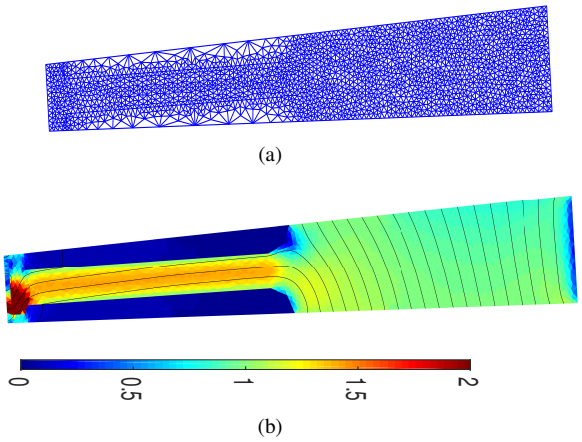

(a)

(b)

Fig. 5. (a) Highly dense first order mesh (b) Magnetic flux density at 35^{th} timestep.

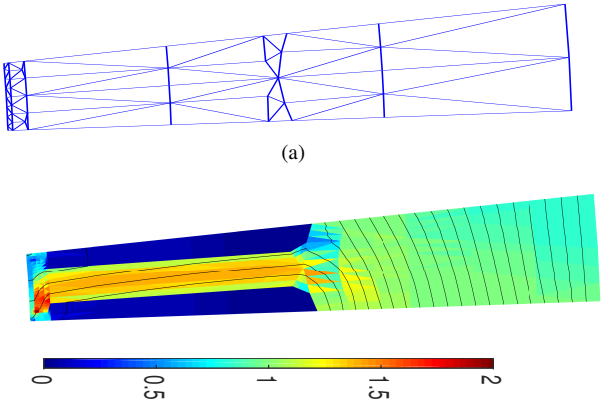

(a)

(b)

Fig. 6. (a) Third order mesh (b) Magnetic flux density at 35^{th} timestep.

effect. Dirichlet boundary conditions and source currents are applied to the studied meshes. The mesh properties are listed in Table I. The meshes of studied stator tooth are shown in Figs. 5a , 6a and, 7a. Further, it should be noted that in general 4-5 different material layers of 0.5 mm-1 mm width of first order elements are normally introduced near the cut-edge [4], [6], [7]. Therefore, the first order reference mesh presented here can be treated as a reasonable mesh to model the presented cutting effect.

$$E_t = \frac{\sqrt{\sum_{el=1}^{N}[(A^h_{el,t} - A^1_{el,t})\Omega_{el}]^2}}{\sqrt{\sum_{el=1}^{N}(A^1_{el,t}\Omega_{el})^2}} \tag{10}$$

$$G = \frac{\sqrt{\sum_{t=1}^{400} E_t^2}}{400} \tag{11}$$

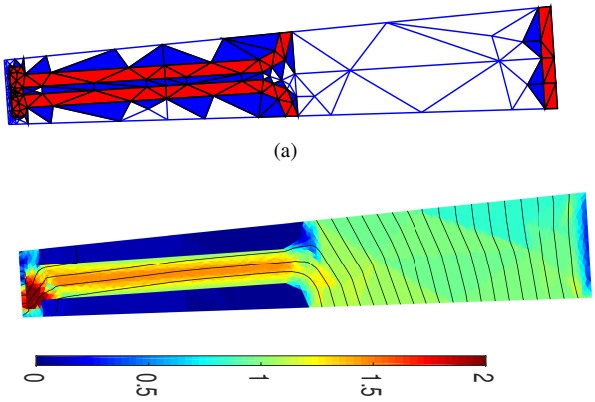

(a)

(b)

Fig. 7. (a) Mixed order mesh. First order, second order and, transition element T_{e1} are shown by white, red and, blue colors respectively. There is no transition element T_{e2} in the presented mesh. (b) Magnetic flux density at 35^{th} timestep.

Two sinusoidal voltage supply periods of 200 time steps per period were studied. As part of the result, we obtain the magnetic vector potential in the discretized solution domain. The calculated magnetic flux density distribution at 35^{th} time step was also plotted in Figs. 5b, 6b and, 7b. The error at a time step E_t (10) and, the average error across all time steps G (11) are calculated. The magnetic vector potential solution of the reference first order mesh at the centroid of the element el is presented as $A^1_{el,t}$ and the one at the same geometric location with the corresponding mixed order mesh solution is $A^h_{el,t}$. Ω_{el} is the area of the element el. G was approximately $2.96 \cdot 10^{-4}$ for the studied mixed order elements based stator tooth case. Moreover, similar error magnitude (G=$2.84 \cdot 10^{-4}$) was observed in the third order mesh.

C. Time harmonic model of induction machine

As the comparative analysis of a stator tooth with the mixed order elements was found satisfactory, a case with the complete machine geometry was also analyzed. The motor data is presented in Table II. The selected meshes of first order, third order and, mixed order elements are shown in Figs. 8a, 8b and, 8c. The mesh data is specified in Table III. We can observe a progressive decrease in the number of nodes of first order, third order and mixed order element meshes.

TABLE II
MOTOR DATA

Shaft Power	37 kW
Voltage	400 V
Frequency	50 Hz
Connection	Star
Pole pairs	2
Stator outer diameter	310 mm
Stator inner diameter	200 mm
Air gap	0.8 mm
Number of stator slots	48
Number of rotor slots	40

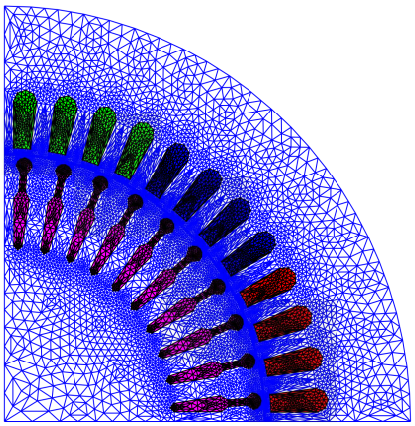

(a)

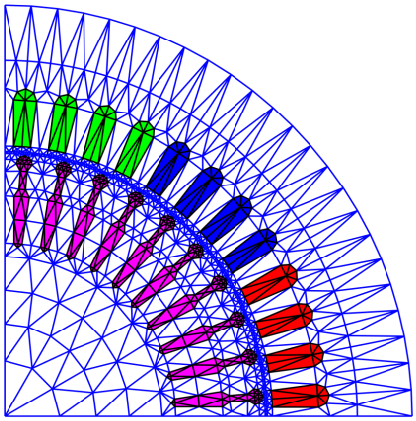

(b)

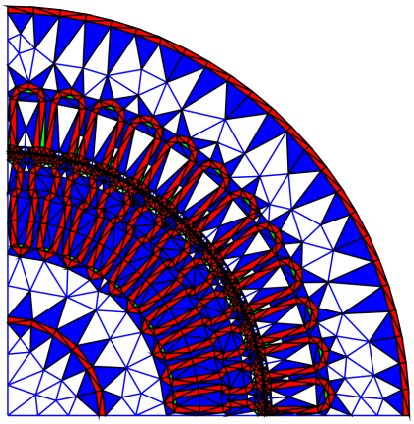

(c)

Fig. 8. (a) Dense first order mesh for induction machine. (b) Third order mesh for induction machine. (c) Mixed order mesh for induction machine. First order, second order, transition elements T_{e1} and T_{e2} are shown by white, red, blue and green colors respectively.

The time harmonic analysis was carried out for no load and full load cases and the machine performance parameters such as stator current and torque were calculated. The distribution of magnetic flux density at full load with the mixed order elements is presented in Fig. 9. It is clear from the simulation results of the stator tooth as well as the full machine that cutting changes the magnetic flux desnity distribution near the cut edge. The summary of results is presented in Table IV and Table V. As a result of the permeability deterioration due to the cutting, the magnetizing current has increased in the no load case. The core losses at 50 Hz were calculated based on (6). A clear increase in the core losses can also be observed in both no load and full load cases. There was a relatively minor decrease in the torque of the machine due to cutting.

TABLE III
MESH DATA

Mesh	Elements	Nodes
First Order	17328	8717
Third order	1516	6901
Mixed order	1982	2737

TABLE IV
TIME HARMONIC SIMULATION AT NO LOAD

Parameter	Nondegraded	Degraded	%Difference
Stator Current (A)	28.1	28.7	2.3
Stator Core Loss (Mixed order) (W)	144.	159.2	10.4
Stator Core Loss (Third order) (W)	143.0	159.0	11.2
Stator Core Loss (First order) (W)	143.5	159.2	11.0

TABLE V
TIME HARMONIC SIMULATION AT FULL LOAD

Parameter	Nondegraded	Degraded	%Difference
Stator Current (A)	70.4	70.6	0.3
Torque (Nm)	250.6	250.3	-0.1
Stator Core Loss (Mixed order) (W)	138.2	152.8	10.5
Stator Core Loss (Third order) (W)	137.2	152.8	11.4
Stator Core Loss (First order) (W)	137.6	153.0	11.2
Slip	0.0135	0.0135	

TABLE VI
ERROR IN TIME HARMONIC SIMULATION

Parameter	No load Nonde-graded	No load Degraded	Full load Nonde-graded	Full load Degraded
Magnetic Vector Potential (Mixed)	$1.2 \cdot 10^{-2}$	$1.3 \cdot 10^{-2}$	$1.5 \cdot 10^{-2}$	$1.6 \cdot 10^{-2}$
Stator Current (Mixed)	$3.4 \cdot 10^{-2}$	$3.3 \cdot 10^{-2}$	$5.4 \cdot 10^{-3}$	$2.5 \cdot 10^{-3}$
Magnetic Vector Potential (Third order)	$2.4 \cdot 10^{-3}$	$3.9 \cdot 10^{-3}$	$4.2 \cdot 10^{-3}$	$5.6 \cdot 10^{-3}$
Stator Current (Third order)	$1.5 \cdot 10^{-2}$	$1.4 \cdot 10^{-2}$	$3 \cdot 10^{-3}$	$6 \cdot 10^{-3}$

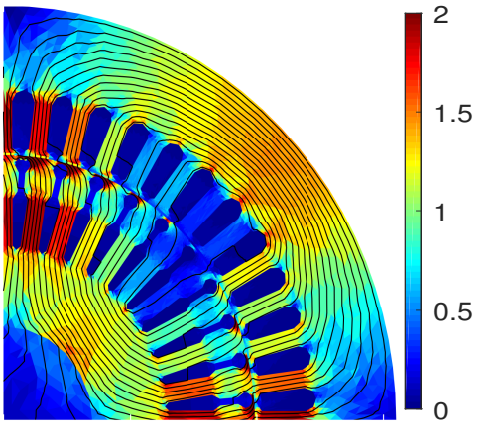

(a)

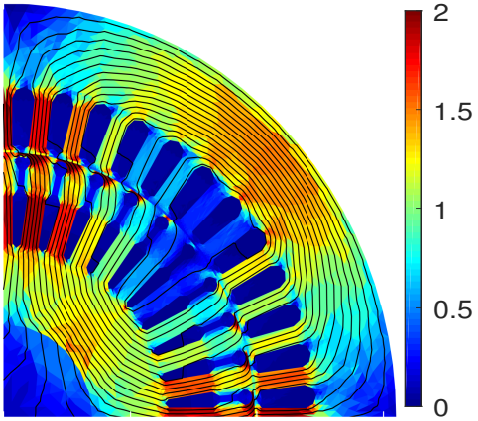

(b)

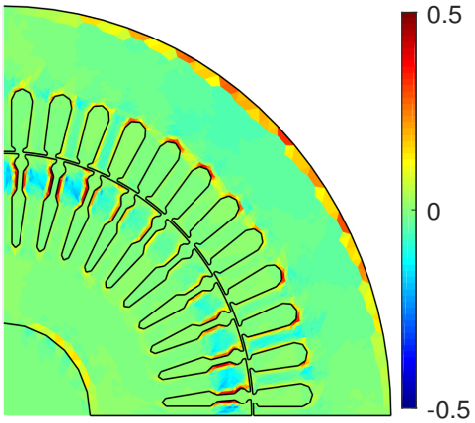

(c)

Fig. 9. Magnetic flux density distribution (a) Without cutting effect (b) With cutting effect (c) Respective difference.

The error in the mixed order element based FEM simulation solution i.e. the real component of the magnetic vector potential (10) and the supply current are calculated and presented in Table VI. Although, the magnitude of the error in the magnetic vector potential is not significant, it is higher than in the stator tooth case. Therefore, the error in the different mesh cases without any cutting effect are also calculated. It seems that the majority of the error in the finite element simulations is generated due the different mesh topologies rather than due

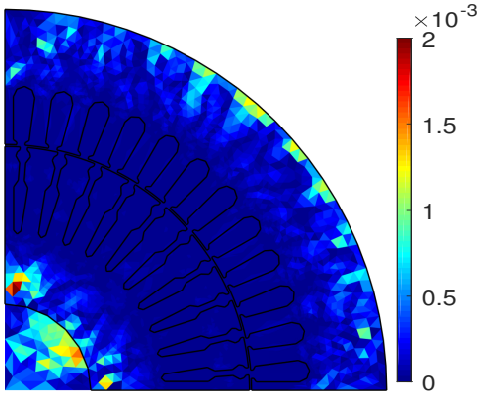

Fig. 10. Spatial distribution of error

TABLE VII
COMPUTATION TIME IN SECONDS

Test cases	First order	Third order	Mixed order
Stator teeth	153	1.31	1.21
Stator teeth (per iteration)	$5.9{\cdot}10^{-2}$	$7.8{\cdot}10^{-4}$	$5.9{\cdot}10^{-4}$
Full machine	310.15	158.47	9.45
Full machine (per iteration)	3.10	1.58	0.94

to cutting effect. Further, the spatial distribution of the error presented in Fig. 10 shows that the respective errors belong to the regions away from the major cutting edges. As a result, the errors in the solution are concluded to be at acceptable level.

D. Computation time

The main aim of the application of the mixed order elements was to reduce the computation time to model the cutting effect. The computation time of the finite element simulation depends on the nature of the resultant linear system of equations. In general, a resultant matrix system with a large number of unknowns and a higher number of non-zero entries results in a higher computation time. With the first order elements, a good sparse system matrix can be obtained however, the number of unknowns will be large. A uniform higher order system will lower the number of unknowns, but the sparseness will be less. Therefore, with the mixed order elements we are able to place higher order elements just where we need; i.e. near the cut edge. This system may result in a good compromise between the number of unknowns and the sparseness of resultant system of equation; thus it may improve the overall computational efficiency. For example, the sparsity (percentage of zeros in the system matrix) in the studied stator tooth case was 99.70 %, 95.43 % and, 96.48 % for the first order, third order and mixed order meshes respectively.

The computation time of the studied meshes was noted with a quad core CPU with maximum processor speed of 3.6 GHz and summarized in Table VII. There are two orders of magnitude decrease in the computation time for the third order

and the mixed order meshes with respect to the dense mesh in the case of stator tooth. Further, the mixed order mesh for the time harmonic case was more than 30 and 15 times faster than the first order and third order meshes respectively. Overall, the mixed order mesh proves to be more efficient than the third order and first order meshes in the context of modeling the cutting effect. Based on the literature, the mesh density of the studied meshes are considered reasonable in this context.

Further, the effect of different meshes on the computation time with the error in the magnetic vector potential is analyzed. For this purpose, four different meshes of first order and four of mixed order were selected. The numbers of nodes of the first-order meshes were 8717, 5178, 4315 and 2552. Similarly, the mixed-order meshes with 7276, 4322, 3067 and 2737 nodes were selected. The obtained solutions from these meshes were compared with a very dense first-order mesh with 15518 nodes. While selecting the mesh densities, care was taken such that highly coarse and highly dense meshes of both types will result in quite similar accuracies with the reference solution. Figure 11 represents the computation time and error in the finite element simulation of the cage induction machine at no-load when the cutting effect was considered. In line with the above presented results, the mixed order meshes prove to be more computationally efficient for the studied case.

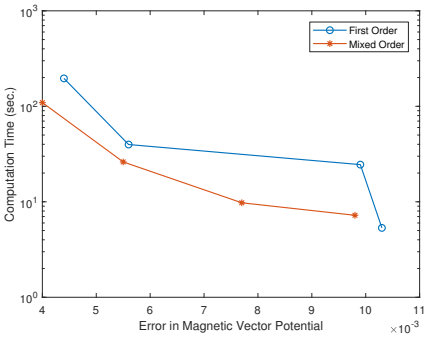

Fig. 11. Computation time and error comparison with first order and mixed order meshes

IV. Conclusion and Future Work

A mixed order based finite element formulation was presented in the context of modeling of cutting related effects in electrical machines. The accuracy of the mixed order elements was found to be within an acceptable range when compared to that of a dense first order mesh of a stator tooth in a time-stepping finite element analysis. Further, a complete machine geometry was also simulated with the presented mixed order finite element formulation and the effect of cutting on the machine performance was discussed. The mixed order elements proved to be more computationally efficient in the simulations.

As part of a future work, a separate mesh layer, just adjacent to the magnetically degraded layer should help in generating more uniform transition elements and subsequently should reduce possible numerical inaccuracies. Further, as the world is moving towards more energy efficient machines, application of efficient techniques such as the mixed order finite elements may motivate machine designers to include the associated cutting effects at the design stage.

Acknowledgment

This research work has received funding from the European Research Council under the European Unions Seventh Framework Programme (FP7/2007-2013) / ERC Grant Agreement n. 339380.

References

[1] H. M. S. Harstick, M. Ritter, and W. Riehemann, "Influence of punching and tool wear on the magnetic properties of nonoriented electrical steel," *IEEE Trans. Magn.*, vol. 50, no. 4, pp. 1–4, April 2014.

[2] G. Pasquarella and J. Schneider, "Electric machine innovation by integrated laser cutting technology," in *Proc. Int. Workshop Magn. Metallurgy, Gent, Belgium*, Sept 2008, pp. 23–24.

[3] M. Hofmann, H. Naumoski, U. Herr, and H. G. Herzog, "Magnetic properties of electrical steel sheets in respect of cutting: Micromagnetic analysis and macromagnetic modeling," *IEEE Transactions on Magnetics*, vol. 52, no. 2, pp. 1–14, Feb 2016.

[4] H. Sano, K. Narita, E. Zeze, T. Yamada, U. Kazuki, and K. Akatsu, "A practical approach for electromagnetic analysis with the effect of the residual strain due to manufacturing processes," in *Proc. 2016 IEEE Energy Conversion Congress and Exposition (ECCE)*, Sept 2016, pp. 1–7.

[5] A. Pulnikov, "Modification of magnetic properties of non oriented electrical steels by the production of electromagnetic devices," Ph.D. dissertation, Dept. Elect. Energy, Syst. and Autom., Ghent University, Ghent, Belgium, 2003–2004.

[6] M. Bali, H. De Gersem, and A. Muetze, "Finite-element modeling of magnetic material degradation due to punching," *IEEE Trans. Magn.*, vol. 50, no. 2, pp. 745–748, 2014.

[7] L. Vandenbossche, S. Jacobs, X. Jannot, M. McClelland, J. Saint-Michel, and E. Attrazic, "Iron loss modelling which includes the impact of punching, applied to high-efficiency induction machines," in *Proc. 2013 3rd International Electric Drives Production Conference (EDPC)*, Oct 2013, pp. 1–10.

[8] A. Cavagnino, R. Bojoi, Z. Gmyrek, and M. Lefik, "Stator lamination geometry influence on the building factor of synchronous reluctance motor cores," *IEEE Trans. Ind. Appl.*, vol. 53, no. 4, pp. 3394–3403, July 2017.

[9] T. P. Holopainen, P. Rasilo, and A. Arkkio, "Identification of magnetic properties for cutting edge of electrical steel sheets," *IEEE Trans. Ind. Appl.*, vol. 53, no. 2, pp. 1049–1053, March 2017.

[10] M. Bali, H. D. Gersem, and A. Muetze, "Determination of original non-degraded and fully degraded magnetic properties of material subjected to mechanical cutting," *IEEE Trans. Ind. Appl.*, vol. 52, no. 3, pp. 2297–2305, May 2016.

[11] R. Sundaria, A. Lehikoinen, A. Hannukainen, and A. Arkkio, "Higher-order finite element modeling of material degradation due to cutting," presented at IEEE Int. Electric Machines and Drives Conf. (IEMDC), Miami, USA, 2017.

[12] L. Demkowicz, *Computing with hp-Adaptive Fintie Elements: Volume 1: One and Two Dimensional Elliptic and Maxwell Problems*. Chapman and Hall/CRC, 2006.

[13] C. Schwab, *p- and hp- Finite Element Methods*. Clarendon Press, 1998.

[14] D. Giannacopoulos and S. McFee, "Towards optimal h-p adaptation near singularities in finite element electromagnetics," *IEEE Trans. Magn.*, vol. 30, no. 5, pp. 3523–3526, Sept 1994.

[15] P. Dular, J. Y. Hody, A. Nicolet, A. Genon, and W. Legros, "Mixed finite elements associated with a collection of tetrahedra, hexahedra and prisms," *IEEE Trans. Magn.*, vol. 30, no. 5, pp. 2980–2983, Sept 1994.

[16] A. Arkkio, "Analysis of induction motors based on the numerical solution of the magnetic field and circuit equations," Ph.D. dissertation, Laboratory of Electromechanics, Helsinki Univ. of Tech., Espoo, 1987.

[17] A. Arkkio, "Finite element analysis of cage induction motors fed by static frequency converters," *IEEE Trans. Magn.*, vol. 26, no. 2, pp. 551–554, Mar 1990.

Ravi Sundaria was born in August 1990. He received the B.Tech. degree from Malaviya National Institute of Technology, Jaipur, India, in 2012 and M.Sc. (Tech.) degree from Aalto University, Espoo, Finland, in 2016 with specialization in electrical machines and drives. He is currently working toward the Ph.D. degree at Aalto University.

He worked at Maruti Suzuki India Limited for two years as part of electrical project group. His current research interests include numerical modeling and structural optimization of electrical machines with specific consideration to manufacturing related losses.

Antti Lehikoinen was born in Joensuu, Finland, in 1988. He received the M.Sc. (Tech.) and D.Sc. (Tech.) degrees in electromechanics from the School of Electrical Engineering, Aalto University, Espoo, Finland, in 2013 and 2017, respectively, where he is currently working as postdoctoral researcher.

His current research interests include stochastic modeling and prediction of additional losses due to circulating currents in random-wound machines.

Antti Hannukainen was born in Pori, Finland 1981. He received the M. Sc. (Tech) and D. Sc. (Tech) degrees from the Department of Electrical Engineering, Helsinki University of Technology and Department of Mathematics, Aalto University, Espoo, Finland, in 2007 and 2011 respectively.

He has worked as a researcher at RWTH Aachen in Germany, as a visiting researcher at the Vienna University of Technology in Austria, and as Academy of Finland postdoctoral researcher at Department of Mathematics and Systems Analysis, Aalto University, Finland. Since 2014, he is an assistant professor at the Department of Mathematics and System Analysis, Aalto University. His research interest are in problems related to electromagnetics and the efficient solution of the large linear systems related to the finite element method with a focus on preconditioned iterative solution methods and the analysis of their convergence properties. In addition, his research includes, among others, the modelling of laminated structures using homogenization.

Antero Arkkio was born in Vehkalahti, Finland, in 1955. He received the M.Sc. (Tech.) and D.Sc. (Tech.) degrees from the Helsinki University of Technology, Espoo, Finland, in 1980 and 1988, respectively.

He is currently a Professor of Electrical Engineering with Aalto University, Espoo. His current research interests include modeling, design, and measurement of electrical machines.

Anouar Belahcen (M13SM15) was born in Morocco, in 1963. He received the B.Sc. degree in physics from the University Sidi Mohamed Ben Abdellah, Fes, Morocco, in 1988, and the M.Sc. (Tech.) and Dr. (Tech.) degrees from the Helsinki University of Technology, Espoo, Finland, in 1998, and 2004, respectively.

From 2008 to 2013, he was an Adjunct Professor in coupled problems and material modeling with Aalto University, Espoo. Since 2011, he has been a Professor of Electrical Machines with the Tallinn University of Technology, Tallinn, Estonia. In 2013, he became a Professor of Energy and Power with Aalto University. His current research interests include numerical modeling of electrical machines, especially magnetic material modeling, coupled magnetic and mechanical problems, magnetic forces, and magnetostriction.